Polarization rotator for shear elastic waves

Cite as: Appl. Phys. Lett. **121**, 042201 (2022); https://doi.org/10.1063/5.0090261
Submitted: 04 March 2022 • Accepted: 09 July 2022 • Published Online: 26 July 2022

Yuqi Jin, Teng Yang, Tae-Youl Choi, et al.

Applied Physics Letters ARTICLE scitation.org/journal/apl

Polarization rotator for shear elastic waves

Cite as: Appl. Phys. Lett. **121**, 042201 (2022); doi: 10.1063/5.0090261
Submitted: 4 March 2022 · Accepted: 9 July 2022 ·
Published Online: 26 July 2022

Yuqi Jin,[1,2] Teng Yang,[2,3] Tae-Youl Choi,[4] Narendra B. Dahotre,[2,3] Arup Neogi,[5,a)] and Arkadii Krokhin[1,a)]

AFFILIATIONS

[1]Department of Physics, University of North Texas, Denton, Texas 76203, USA
[2]Center for Agile and Adaptive Additive Manufacturing, University of North Texas, Denton, Texas 76207, USA
[3]Department of Materials Science and Engineering, University of North Texas, Denton, Texas 76207, USA
[4]Department of Mechanical Engineering, University of North Texas, Denton, Texas 76207, USA
[5]Institute of Fundamental and Frontier Sciences, University of Electronic Science and Technology of China, Chengdu 611731, People's Republic of China

Note: This paper is part of the APL Special Collection on Acoustic and Elastic Metamaterials and Metasurfaces.
[a)]**Authors to whom correspondence should be addressed:** arkady@unt.edu and arup@uestc.edu.cn

ABSTRACT

We designed and characterized a 3D printed acoustic shear wave polarization rotator (PR) based on the specific nature of the fused-deposition-modeling printing process. The principle of the PR is based on rotation of the polarization axis of a shear wave due to the gradual change in orientation of the axis of anisotropy along the direction of wave propagation of a printed layered structure. The component of the shear modulus parallel to the infilled lines within each layer is significantly higher than that in the perpendicular direction. As the PR was printing, a small angle between neighboring layers was introduced, resulting in a 3D helicoidal pattern of distribution of the axes of anisotropy. The polarization of the propagating shear wave follows this pattern leading to the rotation of the polarization axis by a desirable angle. The total rotation angle can be tuned by the number of printed layers. The fabricated 90° rotators demonstrate high performance that can be improved by changing the infill fraction settings.

Additive manufacturing (AM)[1,2] has undergone development and improvement for decades. Major technique categories in AM that are widely used in industrial fields[3] and research projects include plastic filament reformatting, liquid resin curing, and metal powder melting. These categories are often combined with the most commonly applied printing processes of FDM,[4] stereolithography,[5] and selective laser melting.[6] Digital printing,[7] inkjets,[8] and solid-state metal/alloy printing[9] are examples of recently developed printing techniques for current applications, and printable materials contain groups such as polymers,[10] ceramics,[11] metal/alloys,[12] and even composites.[3,13]

Although the mechanical properties of materials produced using the current AM processes are inferior to conventionally manufactured products,[14] the flexibility of AM techniques drives the interest in improvement and further investigation for next-generation manufacturing technology. Customized structures of the complex geometric shape with specific material combinations that may be infeasible, cost-prohibitive, and/or very challenging to realize by conventional, subtractive manufacturing processes can be readily fabricated using AM. Additionally, unlike any other known manufacturing techniques, the unconventional methods of additive manufacturing allow the nature of the printing process to be used to design specific applications and devices.

Manipulation of the various process parameters and mechanisms can produce structures with a very wide range of mechanical and physical properties from the same printing tool. For example, in laser-melting-based AM techniques, ultrafine grain structures,[1] alignment of anisotropic mechanical properties,[15] and internal twinning textures[16] were obtained without any additional post-processes. In direct energy deposition printers, dissimilar metals that are immiscible were joined together using a thin barrier material.[17] Friction stir, another AM processing method, was used for local reconstruction of an existing complex structure.[18] Motivated by these modern manufacturing process-based structures, we have utilized the nature of FDM printing to design a shear wave polarization rotator (PR).

A metamaterial-based polarization rotator for linearly polarized electromagnetic waves of the terahertz region has been proposed and fabricated in Ref. 21. It contains a tri-layer metasurface of thin metal plates separated by a dielectric. Each plate has parallel narrow slits, resulting in a strong anisotropy in transmitting electromagnetic waves with parallel or perpendicular polarization. The plates are rotated by

45° relative to each other. This metasurface serves as a highly efficient 90° polarization rotator. Unlike electromagnetic waves, transverse by nature, transverse acoustic waves cannot propagate through fluid media due to the lack of an elastic shear modulus. In solids, rotation of a shear wave oscillation plane can be realized by applying phased array systems and complex metamaterials.[19,20] The fabrication of these metamaterial designs is quite complex, making their practical use cost-prohibitive. On the contrary, rotation of a shear wave polarization axis merely needs a sufficient level of anisotropy of the shear modulus of the elastic media.

The line-by-line printed FDM process provides high anisotropy of the shear modulus within a printed layer. The axis of anisotropy gradually rotates from layer to layer by an appropriate adjustment of the printing direction. The polarization axis of a shear wave propagating along the layered structure follows the direction of the local axis of anisotropy, thus realizing the global rotation of the polarization axis. In the case of elastic waves, a multilayered structure is necessary to rotate the polarization axis effectively. Note that polarization of light occurs in organic polymers with long-chain molecules. Due to strong anisotropy, such dichronic polarizers exhibit transparency for a light wave with certain polarization and strong suppression for the waves with perpendicular polarization. Here, we explore the principle of operation of optical dichronic polarizers for polarization of elastic waves. A set of elastically anisotropic 3D printed layers, forming a helical structure, serve as an effective rotator for elastic shear waves.

In this paper, we report a layered design of acoustic PR that takes advantage of the nature of the FDM 3D printing process. The proposed polarizer can be used as a filter or insulator of the transversal component of an elastic wave having both transversal and longitudinal displacements. Examples of such waves are the Rayleigh or Lamb wave or any other elastic wave propagating in a finite size sample. The transverse component of a mixed wave can be easily filtered out by the polarizer, leaving pure longitudinal vibrations for further analysis. An obvious advantage of this filtering is its nondestructive nature.

A cylindrical-shaped transverse acoustic 90° PR shown schematically in Fig. 1 was fabricated using an FDM printer. A stack of layers printed with a small angular shift relative to each other, as shown in Fig. 1(d), represents PR for shear waves. It is known that the shear modulus in a straight-line infill FDM printed product has the maximum (minimum) value when the applied deformation was along (across) the infilled line direction.[22] In addition, the infill fraction is another factor that highly deviates the elastic constant.[23,24]

The performance of the FDM acoustic polarizer was experimentally characterized by measuring the transmission of the shear wave propagating from left to right using a pair of shear-wave transducers serving as emitter and receiver. Figure 1 illustrates the experimental setup along with the configuration for the transmission between the transducers and the geometry required for the anisotropy of the multilayered rotator. The proposed FDM acoustic polarizing rotator is realized by tuning horizontal oscillations of the shear wave to vertical oscillations. Additionally, a parametric study was performed to optimize the transmission and the efficiency of rotation of the axis of polarization of shear waves.

In this work, all the polarizer samples were printed by PolyPrinter 229 single extruder FDM printer illustrated in Fig. 1(b). We used black ABS (Acrylonitrile Butadiene Styrene) filament from

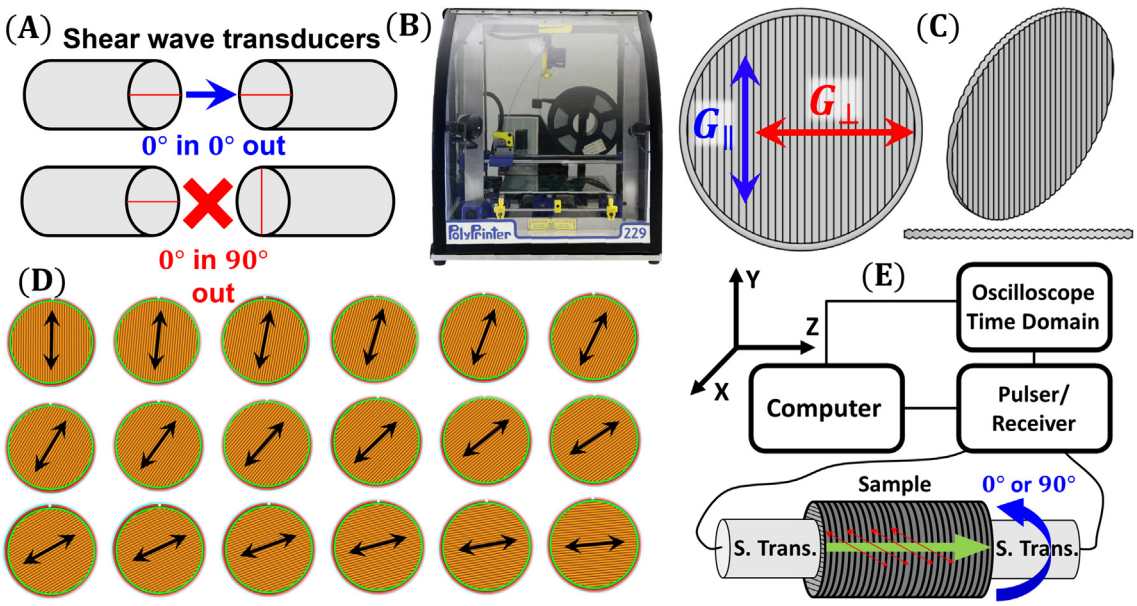

FIG. 1. Principal scheme of the polarization rotator: (a) Mutual orientation of emitting/detecting shear wave transducers. Emitted source signal freely propagates through an isotropic sample and is detected by the receiver if both transducers are parallel, but not if transducers are orthogonal. (b) The FDM 3D printer, PolyPrinter 229, used in the experiment. (c) Top and side views of the anisotropic pattern in a layer of FDM structure with line infill. The shear modulus is higher in the direction perpendicular to the infilled lines than in the parallel direction, $G_{\perp} \gg G_{\parallel}$. (d) The infill line orientations were gradually rotated during the printing process from the bottom (left-upper) to the top layer (right-lower), providing total rotation by 90°. (e) Experimental setup for bistatic transmission measurements through a printed polarization rotator. The emitted transducer excites shear wave with horizontal polarization. The receiving transducer can be rotated to detect the signal with horizontal or vertical polarization.

Hatchbox. The static and dynamic elasticities were characterized by tensile tests and elastography techniques.[22] All the polarizer samples were designed into a cylindrical shape by the Autodesk inventor software. The cylindrical 3D models were then input into the slicing software Ultimaker and converted to G-Code for printing. The sliced models all have one loop of skin with a thickness of 0.4 mm. The pattern of infilled straight lines is shown in Fig. 1(c). It corresponds to uniaxial anisotropy with significant contrast $G_\perp \gg G_\parallel$ ($E_\perp \ll E_\parallel$) between the shear (Young) modulus along the infilled lines $G_\parallel$ ($E_\parallel$) and across the infilled lines $G_\perp$ ($E_\perp$).[22] The infilled percentage was set to 100%, which offered center-to-center space of about 0.32 mm between the neighboring infilled lines.

The gradient rotation angle of the infilled line between each layer [see Fig. 1(d)] was manually introduced into the setting section of the slicing software. The bottom layer in the FDM polarizer was always set to 0° and the top layer to 90°. In parametric study 1, we have printed the polarizer sample with rotational angle intervals of 5°, 3°, and 1°. In parametric study 2, we printed polarizer samples with 1° rotational angle intervals and different infilled line spacing controlled by changing the setting of infill percentages. The infilled percentage of the printed polarizer samples was varied from 100% to 80% to change the contrast between $G_\parallel$ and $G_\perp$. Several reference samples were also printed with parallel orientation of the printed lines to evaluate energy losses.

A 0.4 mm copper nozzle was installed at the printer. The extruding temperature was set to 260 °C for the first layer and 255 °C for the upper layers. The temperature of the heated printing substrate was maintained at 110 °C. The printing speed of samples was $v_T = v_0 = 400$ mm/min, where v_T is the XYZ translation motor speed and v_0 is the extruder motor speed. At the 100% infilled setting, the slicing software programmed the infilled line spacing at 0.32 mm. While decreasing the fill fraction from 100% to 80%, the spacing between infilled lines was increased to 0.4 mm. In parametric study 2, the variance of infilled percentage was from 100% to 80% with a 2.5% interval.

The bistatic acoustic transmission experiments were conducted to characterize the performance of the proposed FDM acoustic PR. A pair of 5 MHz shear wave contacting transducers with a 0.125-in. diameter (Olympus V157) were used in the experiments. Two transducers were aligned and horizontally fixed on an optical table before performing the experiments. One of the transducers excites the broadband pulses within the 3–7 MHz range and a repetition rate of 2 ms, which is incident on one of the ends of the printed samples [see Fig. 1(e)]. Another shear wave transducer was placed on the opposite end of the sample to detect the transmitted signal. The amplitude of shear waves was sufficiently small to ensure the linear regime of propagation. Initially excite shear wave is linearly polarized. Propagating through the helical layered structure it remains linearly polarized, but the axis of vibrations gradually rotates.

Following the study carried out in Ref. 23, we used honey as a coupling material. Since shear waves decay exponentially in viscous fluid, the thickness of the honey layer was comparable to the thickness of the boundary viscous layer $\delta = \sqrt{\eta/2\rho\omega} \approx 0.3$ mm (where η and ρ are the viscosity and density of honey), thus providing strong coupling. The efficiency of honey as a coupling material was compared to that with glycerin and drilling oil in the transducer-to-transducer transmission tests. Honey exhibited the best coupling strength.

The internal trigger and source signal were from a JSR Ultrasonic DPR 500 Pulse/Receiver. The acoustic wave was collected from the receiver transducer and sent to the pulse receiver. A 1 MHz high-pass filter and 10 MHz low-pass filters were applied to the detected signal. The filtered signal was then passed to an oscilloscope, Tektronix MDO 3024b. The oscilloscope averaged 512 signals for each measurement and acquired the data. The sampling rate was set at 2 GHz. The total recorded temporal length was 0.2 ms and remained constant in all the measurements. In the experiments, we defined unpolarized transmission as 0°-in 0°-out. The polarized transmission is referred to as 0°-in 90°-out. In the measurements, the emission source transducer was always placed at 0°. The oscillation direction was aligned to the infilled direction on the incident surface of the printed samples. The receiver transducer was aligned in the appropriate orientation relative to the source transducer to measure the 0°-in and 0°-out signal. For 0°-in 90°-out measurements, the receiver transducer was rotated by 90° around the cylindrical axis.

In a bistatic configuration of two single-element shear transducers, an acoustic signal can hardly be detected when the emitting and receiving transducers are oriented mutually perpendicular. The transmission measurements through a practically uniform and isotropic molded ABS plastic slab are shown in Fig. 2(a) for parallel and perpendicular orientation of the transducers. The averaged over frequency amplitude ratio $A_{0^\circ\to90^\circ}/A_{0^\circ\to0^\circ}$ was as small as 0.008. Small transmission for perpendicular orientation is due to some residual stresses and imperfect uniformity of the molded ABS sample.

The efficiency of ideal multilayered PR can be easily evaluated. Consider the polarization vector to rotate by α° for a wave that is transmitted through a single layer. Under the conditions of strong coupling between the homogeneous layers, the amplitude of the shear wave oscillating parallel to the printed lines, which initially was A_0, slightly decreases and becomes $A_1 = A_0 \cos\frac{\pi\alpha}{180}$. On passing through n layers of the material, the wave polarization vector rotates by $n\alpha^\circ$, and the amplitude decreases to $A_n = A_0 \cos^n\frac{\pi\alpha}{180}$. A full wave-plate, i.e., a rotation of the wave by 90°, requires a rotator composed of $n = 90/\alpha$ layers. In an efficient rotator $\frac{\pi\alpha}{180} \ll 1$ and the amplitude ratio yields

$$\frac{A_{0^\circ\to90^\circ}}{A_0} \approx 1 - \frac{\pi^2}{720}\alpha. \tag{1}$$

Thus, the efficiency of ideal PR decreases linearly with α, i.e., in practice, the angle between printed lines in the neighboring layers cannot exceed a few degrees. In a real sample, each layer is a source of losses caused by reflection, scattering, and dissipation, which are neglected in Eq. (1). Each PR depends on the properties of the printing material and should be calibrated for the specific number of layers and their thickness for the optimum extinction ratio.

We conducted several experiments with the FDM printed acoustic PRs with 100% infill setting and different angles α. In Fig. 2(b), we present the temporal signals transmitted through the PR with $\alpha = 5^\circ$ (red line) and through the reference sample with $\alpha = 0^\circ$ containing the same number of layers (blue line). A rotation of the anisotropy axis leads to about two orders of magnitude increase in the ratio $\frac{A_{0^\circ\to90^\circ}}{A_{0^\circ\to0^\circ}} = 0.66$, as compared to a homogeneous plastic slab, where $\frac{A_{0^\circ\to90^\circ}}{A_{0^\circ\to0^\circ}} = 0.008$. Since for $\alpha = 5^\circ$ Eq. (1) gives $\frac{A_{0^\circ\to90^\circ}}{A_{0^\circ\to0^\circ}} = 0.93$, the efficiency of the fabricated PR is 0.66/0.93 = 71% of its theoretical value.

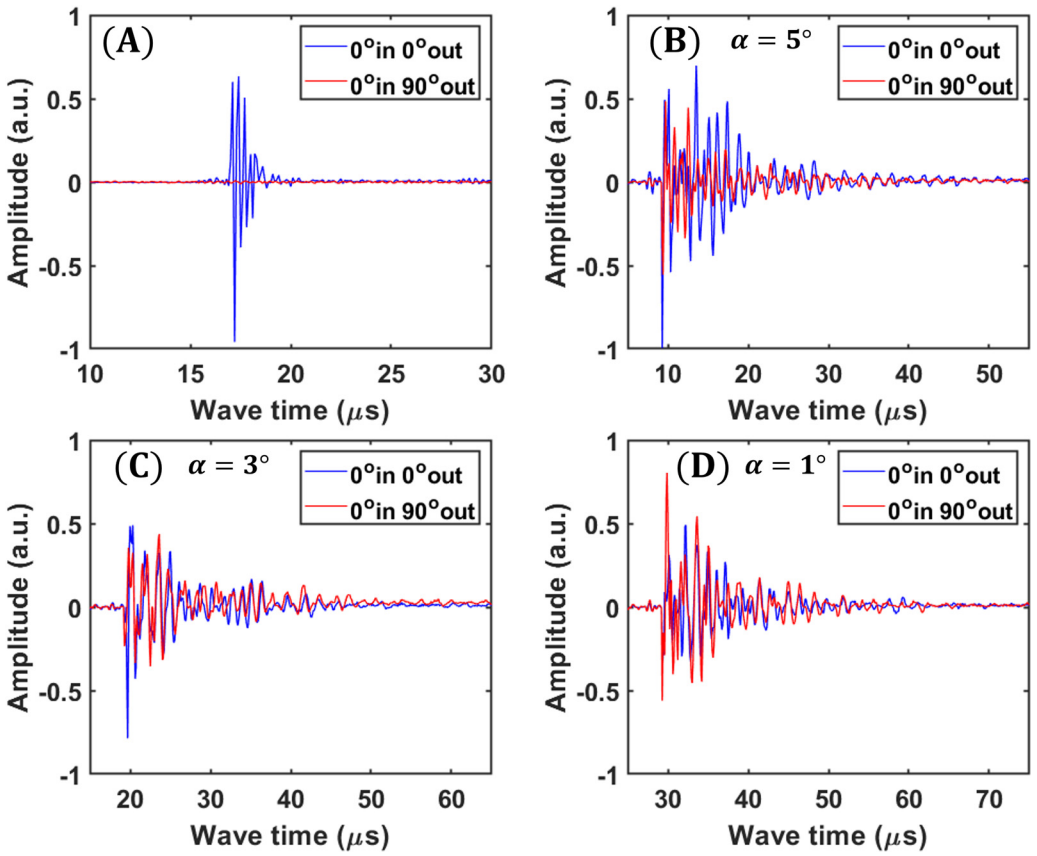

FIG. 2. Transmission of shear wave pulses through different fabricated samples. (a) Transmissions through a uniform and isotropic ABS slab obtained by the molding process. (b) Transmissions through the printed PR with $\alpha = 5°$. (c) Transmissions through the printed PR with $\alpha = 3°$. (d) Transmissions through the printed PR with $\alpha = 1°$. Here, 0°-in 0°-out (0° in 90°) transmission refers to excitation of oscillations parallel to the infilled line direction on the first layer of the PR, and the same (perpendicular) orientation of the receiver.

The main source of losses is a stronger reflection between the layers with nonparallel printed lines than similar layers with parallel lines.

Such multiple reflections not only reduce the amplitude of the signal but also lead to phase shifts since the positions of the peaks in Fig. 2(b) do not coincide. Because of the multilayered structure and natural absorption in the material, there is expected attenuation of the signal transmitted through the reference sample, i.e., $A_{0°\to0°} \ll A_0$. One more source of attenuation is frequency dispersion of sound velocity. However, these losses are irrelevant to the rotation process of the polarization axis, and they should be excluded from the evaluation of efficiency.

Frequency dispersion of sound and energy losses accumulated during pulse transmission through the sample are the main sources of attenuation of the peak amplitudes of the transmitted signal. Hence, the polarization performance was not characterized by the conventional output/input ratio, which is usually small even for the pulse transmitted without rotation of the polarization axis ($\alpha = 0$), see Fig. 3(c). Unlike this, the relative amplitude $\frac{A_{0°\to90°}}{A_{0°\to0°}}$ contains mostly the information about the efficiency of the polarization axis rotation. To account for frequency dispersion, each amplitude $A_{0°\to90°}$ and $A_{0°\to0°}$ is obtained by averaging the absolute value of the maximum and minimum peaks, detected in the time-of-flight measurements.

Two more PR with finer resolutions, $\alpha = 3°$ and 1°, have been printed to demonstrate higher efficiency. The transmission spectra are shown in Figs. 2(c) and 2(d). For the device with $\alpha = 3°$, the ratio of amplitudes $\frac{A_{0°\to90°}}{A_{0°\to0°}} = 0.87$ is close to its theoretical maximum of 0.96 given by Eq. (1). The efficiency of this PR is only 9% less than the theory predicts. For the PR with $\alpha = 1°$, the theoretical efficiency ≈ 0.99 is close to unity. In the experiment, we observed that several signal peaks with a polarization axis rotated by 90° exceeding the corresponding amplitudes of the signal transmitted through the reference sample. On average, the ratio $\frac{A_{0°\to90°}}{A_{0°\to0°}}$ was indistinguishable from 1. Thus, for the proposed scheme, the increase in the length of the device still is not a sufficiently strong negative factor to overcome the positive effect of a decrease in one-step rotation up to the value of 1°. In the longer rotator, the amplitude of the output signal expectedly becomes weaker relative to the input signal. However, the relative amplitude $\frac{A_{0°\to90°}}{A_{0°\to0°}}$ continues to grow. This tendency is in line with the decrease in the phase shifts between the signals transmitted through the PR and the corresponding reference sample.

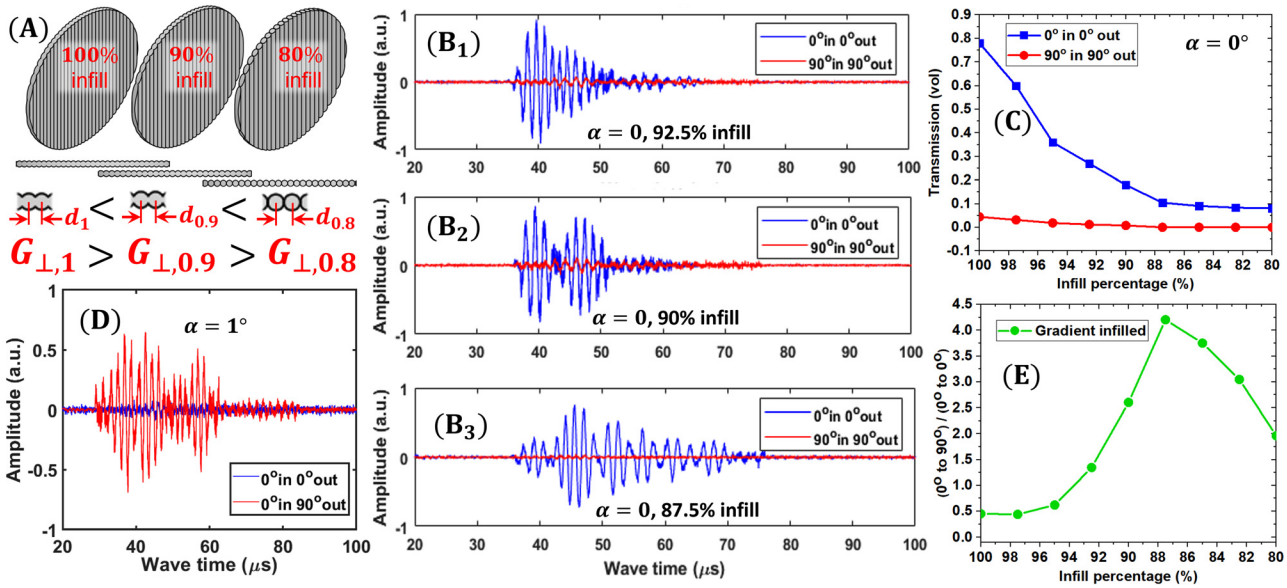

FIG. 3. Optimization of the PR over infill percentage. (a) Lower infill corresponds to larger spacing between the printed lines that reduces the shear modulus of the strucrure. (b) Transmissions of shear wave pulses through three reference samples with $\alpha = 0^\circ$ and different fills. Transmission of shear waves with polarization perpendicular to the printed lines is strongly suppressed. Note a region with lower amplitude of the pulse in (b_2), which is probably related to the bandgap in the spectrum of the periodic layered structure. (c) Decay of the amplitude of the pulses transmitted through the refernce samples with gradually decreasing fill. (d) Transmissions through the PR with $\alpha = 1^\circ$. The amplitude of the signal with polarization axis rotated by 90° exceeds the amplitude of the signal propagating through the PR without rotation of polarization axis. (e) Normalized amplitude of the transmitted signal with 90° rotated polarization vs infill percentage. The maximum transmission was observed at 85% fill.

The proposed PR requires elastic anisotropy within each printed layer. The degree of anisotropy can be optimized by changing the center-to-center distance d between the infilled lines. The resistivity of a printed layer to deformation parallel as well as perpendicular to the lines decreases when this distance increases, see Fig. 3(a). Also, the coupling between the neighboring layers becomes weaker. Although these changes always reduce the amplitudes of the transmitted signals, our experiments show that the polarization contrast performance of the PR can be improved.

Figure 3 presents the transmission spectra for several PRs with differing infill parameters and without the skin lines. The center-to-center infill line spacing cannot be directly varied with the slicing software that was being used. Instead, the spacing can be changed by changing the setting value on the infill percentage. In this study, we varied the infill percentage setting from 100% to 80% in 2.5% intervals, leading to the variance in the center-to-center infill line spacing from $d = 0.32$ to $d = 0.4$ mm.

The effect of increasing distance d can be directly observed by measuring the transmission spectra for the reference samples with all parallel layers, i.e., with $\alpha = 0^\circ$. For three reference samples with fill 92.5%, 90%, and 87.5%, the transmission was measured for parallel (0° in 0° out, blue curve) and perpendicular (90° in 90° out, red line) orientations of the emitter and receiver with respect to the infill lines. Transmission spectra in Fig. 3(b) demonstrate a gradual decrease in the signal 90° in 90° out with a decrease in the fill, which means stronger suppression of waves with the "wrong" polarization. Since the sequence of parallel layers forms a periodic elastic structure, the transmitted pulses exhibit strong frequency dispersion, leading to spreading of the pulses and even evidence of a bandgap in Fig. 3(b_2). An increase in the center-to-center distance weakens the coupling between the neighboring layers. A gradual decrease in amplitude of the signals with both polarizations transmitted through the reference samples with fill decreasing from 100% to 80% is given in Fig. 3(c).

The red curve in Fig. 3(d) represents transmission with 90° rotation of the polarization axis. The rotator contains 90 printed layers oriented at the angle $\alpha = 1^\circ$ with respect to each other. The infill settings were reduced to 87.5%. The transmitted signal was measured by a receiver rotated by 90° (0° in 90° out, red curve) and by 0° (0° in 0° out, blue curve) with respect to the emitter. The signal with rotated polarization turns out to be much stronger. Comparison with the spectra presented in Fig. 2, where the signals have approximately equal amplitudes, leads to a conclusion that a reasonable decrease in center-to-center distance is favorable for the performance of the PR. The estimate [Eq. (1)] for the performance becomes invalid because of the strong reduction of interlayer coupling. Figure 3(e) shows how the amplitude of the transmitted signal with 90° rotation of the polarization axis normalized to the amplitude of the signal passing without rotation changes with infill percentage. Both signals become equal for the fill fraction ≈91%. For smaller fills, the signal with a rotated polarization axis becomes stronger. The maximum is reached at 87.5%, which is the optimal fill for the PR with $\alpha = 1^\circ$. Note that the amplitudes of both signals decay with decreasing fill, but their ratio, which serves as a measure of performance, has a well-pronounced maximum.

Due to strong anisotropy ($G_\perp \gg G_\parallel$) and small value of the angle α, the longitudinal oscillations of a given infill line excite the longitudinal oscillations of the neighboring line. However, since these lines are not exactly parallel, there is an elastic force in the

perpendicular direction that leads to bending deformation and excitation of the flexural mode. This mode provides propagation of the signal in the 0° in 0° out configuration, i.e., the last infill line has a component of displacement vibrating along the direction of vibration of the first infill line. The mechanical coupling between the neighboring lines becomes weaker with lower infill percentage. The off diagonal longitudinal-flexural coupling depends on both elastic moduli, $G_\perp$ and $G_\parallel$, while the diagonal longitudinal–longitudinal coupling depends only on $G_\parallel$. Since $G_\perp$ and $G_\parallel$ decrease with the interline distance, the off diagonal coupling decreases faster when the infill percentage becomes less than 100%. Therefore, the relative amplitude $\frac{A_{0°\to 90°}}{A_{0°\to 0°}}$, grows in Fig. 3(e) when the infill percentage decreases from 100% to 87.5%. Further decrease in the infill percentage is not accompanied by decrease in $G_\perp$, as can be seen from the red curve in Fig. 3(c). The decrease in $G_\parallel$ also becomes much slower for the infill less than 87.5% (see the blue curve). These two factors lead to practically constant off diagonal coupling, while the diagonal coupling continues to drop slowly. This qualitatively explains the maximum in Fig. 3(e)and asymmetric behavior of the efficiency on both sides of the maximum. It is difficult to make a quantitative description since it requires information about an explicit dependence of the coupling tensor on $G_\perp$, $G_\parallel$, infill percentage, angle α, and the details of the interline filling.

In conclusion, we designed and fabricated a polarization rotator for elastic shear waves, using the natural signatures of a FDM 3D printing technique, where the printed pattern appears layer by layer with a nozzle moving along a set of parallel lines. A printed layer possesses elastic anisotropy with a greater shear modulus along the lines. This direction is the natural axis of anisotropy of a printed layer. The rotation of the polarization axis is a multistep process introduced by an incremental angular rotation at each step. When a shear wave passes through a 3D printed layer, the preferential direction of oscillations coincides with the direction of uniaxial elastic anisotropy. The polarization axis of a shear wave passing through a multilayered helicoidal structure follows the direction of the printed lines. The rotation of the polarization axis by the desired angle may be achieved by printing a sufficient number of layers with appropriate rotation steps at each layer. We demonstrated the high efficiency of the proposed polarization rotator containing 90 printed layers, each rotated by 1°. Moreover, the efficiency can be improved by optimization with respect to the parameters of the 3D printing process.

This work was supported by EFRI Grant No. 1741677 from the National Science Foundation. The authors acknowledge the infrastructure and support of the Center for Agile Adaptive and Additive Manufacturing (CAAAM) funded through State of Texas Appropriation No. 190405-105-805008-220.

AUTHOR DECLARATIONS

Conflict of Interest

The authors have no conflicts to disclose.

Author Contributions

Yuqi Jin: Conceptualization (equal); Investigation (lead); Writing – original draft (equal). **Teng Yang:** Data curation (equal); Investigation (equal); Methodology (equal). **Tae-youl Choi:** Data curation (equal); Methodology (lead); Validation (lead); Writing – review and editing (equal). **Narendra B. Dahotre:** Conceptualization (equal); Resources (equal); Supervision (equal); Writing – review and editing (equal). **Arup Neogi:** Project administration (equal); Resources (equal); Supervision (equal); Writing – review and editing (equal). **Arkadii Krokhin:** Formal analysis (equal); Supervision (equal); Writing – review and editing (equal).

DATA AVAILABILITY

The data that support the findings of this study are available on request.

REFERENCES

[1]K. V. Wong and A. Hernandez, "A review of additive manufacturing," Int. Scholarly Res. Not. **2012**, 208760.
[2]T. Yang, S. Mazumder, Y. Jin, B. Squires, M. Sofield, M. V. Pantawane, N. B. Dahotre, and A. Neogi, "A review of diagnostics methodologies for metal additive manufacturing processes and products," Materials **14**(17), 4929 (2021).
[3]S. Mohd Yusuf, S. Cutler, and N. Gao, "The impact of metal additive manufacturing on the aerospace industry," Metals **9**(12), 1286 (2019).
[4]S. Ahn, M. Montero, D. Odell, S. Roundy, and P. K. Wright, "Anisotropic material properties of fused deposition modeling ABS," Rapid Prototyping J. **8**, 248 (2002).
[5]F. P. Melchels, J. Feijen, and D. W. Grijpma, "A review on stereolithography and its applications in biomedical engineering," Biomaterials **31**(24), 6121–6130 (2010).
[6]C. Y. Yap, C. K. Chua, Z. L. Dong, Z. H. Liu, D. Q. Zhang, L. E. Loh, and S. L. Sing, "Review of selective laser melting: Materials and applications," Appl. Phys. Rev. **2**(4), 041101 (2015).
[7]H. Heo, Y. Jin, D. Yang, C. Wier, A. Minard, N. B. Dahotre, and A. Neogi, "Manufacturing and characterization of hybrid bulk voxelated biomaterials printed by digital anatomy 3D printing," Polymers **13**(1), 123 (2020).
[8]G. Cummins and M. P. Desmulliez, "Inkjet printing of conductive materials: A review," Circuit World **38**, 193 (2012).
[9]S. Palanivel, H. Sidhar, and R. S. Mishra, "Friction stir additive manufacturing: Route to high structural performance," JOM **67**(3), 616–621 (2015).
[10]L. J. Tan, W. Zhu, and K. Zhou, "Recent progress on polymer materials for additive manufacturing," Adv. Funct. Mater. **30**(43), 2003062 (2020).
[11]A. Zocca, P. Colombo, C. M. Gomes, and J. Günster, "Additive manufacturing of ceramics: Issues, potentialities, and opportunities," J. Am. Ceram. Soc. **98**(7), 1983–2001 (2015).
[12]D. Herzog, V. Seyda, E. Wycisk, and C. Emmelmann, "Additive manufacturing of metals," Acta Mater. **117**, 371–392 (2016).
[13]F. Hamidi and F. Aslani, "Additive manufacturing of cementitious composites: Materials, methods, potentials, and challenges," Constr. Build. Mater. **218**, 582–609 (2019).
[14]J. J. Lewandowski and M. Seifi, "Metal additive manufacturing: A review of mechanical properties," Annu. Rev. Mater. Res. **46**, 151–186 (2016).
[15]M. V. Pantawane, T. Yang, Y. Jin, S. S. Joshi, S. Dasari, A. Sharma, A. Krokhin, S. G. Srinivasan, R. Banerjee, A. Neogi, and N. B. Dahotre, "Crystallographic texture dependent bulk anisotropic elastic response of additively manufactured Ti6Al4V," Sci. Rep. **11**(1), 633 (2021).
[16]M. V. Pantawane, T. Yang, Y. Jin, S. Mazumder, M. Pole, S. Dasari, A. Krokhin, A. Neogi, S. Mukherjee, R. Banerjee, and N. B. Dahotre, "Thermomechanically influenced dynamic elastic constants of laser powder bed fusion additively manufactured Ti6Al4V," Mater. Sci. Eng., A **811**, 140990 (2021).
[17]H. Rao, R. P. Oleksak, K. Favara, A. Harooni, B. Dutta, and D. Maurice, "Behavior of yttria-stabilized zirconia (YSZ) during laser direct energy deposition of an Inconel 625-YSZ cermet," Addit. Manuf. **31**, 100932 (2020).
[18]R. J. Griffiths, D. T. Petersen, D. Garcia, and H. Z. Yu, "Additive friction stir-enabled solid-state additive manufacturing for the repair of 7075 aluminum alloy," Appl. Sci. **9**(17), 3486 (2019).
[19]Y. Li, X. Jiang, B. Liang, J.-C. Cheng, and L. Zhang, "Metascreen-based acoustic passive phased array," Phys. Rev. Appl. **4**(2), 024003 (2015).

[20]K. Yamashita and M. Okuyama, "Sensitivity improvement of diaphragm type ultrasonic sensors by complementary piezoelectric polarization," Sens. Actuators, A **127**(1), 119–122 (2006).
[21]L. Cong, W. Cao, X. Zhang, Z. Tian, J. Gu, R. Singh, J. Han, and W. Zhang, "A perfect metamaterial polarization rotator," Appl. Phys. Lett **103**, 171107 (2013).
[22]Y. Jin, T. Yang, H. Heo, A. Krokhin, S. Q. Shi, N. Dahotre, T.-Y. Choi, and A. Neogi, "Novel 2D dynamic elasticity maps for inspection of anisotropic properties in fused deposition modeling objects," Polymers **12**(9), 1966 (2020).
[23]R. L. Raer, R. Selfridge, B. T. Khuri-Yakub, G. S. Kino, and J. Souquet, "Contacting transducers and transducer arrays for NDE," in Ultrasonic Symposium, Chicago, IL, 1981.
[24]Y. Jin, E. Walker, H. Heo, A. Krokhin, T.-Y. Choi, and A. Neogi, "Nondestructive ultrasonic evaluation of fused deposition modeling based additively manufactured 3D-printed structures," Smart Mater. Struct. **29**(4), 045020 (2020).